

Model Independent Approach to the Single Photoelectron Calibration of Photomultiplier Tubes

R. Saldanha,^{1,2,3} L. Grandi,^{1,2,3} Y. Guardincerri,^{1,4} and T. Wester³

¹*Kavli Institute for Cosmological Physics, University of Chicago, Chicago, IL 60637, USA*

²*Enrico Fermi Institute, University of Chicago, Chicago, IL 60637, USA*

³*Department of Physics, University of Chicago, Chicago, IL 60637, USA*

⁴*Fermi National Accelerator Laboratory, Batavia, IL 60510, USA*

(Dated: December 3, 2024)

The accurate calibration of photomultiplier tubes is critical in a wide variety of applications in which it is necessary to know the absolute number of detected photons or precisely determine the resolution of the signal. Conventional calibration methods rely on fitting the photomultiplier response to a low intensity light source with analytical approximations to the single photoelectron distribution, often leading to biased estimates due to the inability to accurately model the full distribution, especially at low charge values. In this paper we present a simple statistical method to extract the relevant single photoelectron calibration parameters without making any assumptions about the underlying single photoelectron distribution. We illustrate the use of this method through the calibration of a Hamamatsu R11410 photomultiplier tube and study the accuracy and precision of the method using Monte Carlo simulations. The method is found to have significantly reduced bias compared to conventional methods and works under a wide range of light intensities, making it suitable for simultaneously calibrating large arrays of photomultiplier tubes.

I. INTRODUCTION

Photomultiplier tubes (PMTs) are widely used to detect low levels of light in scientific experiments, medical apparatus and industrial equipment. PMT operation is typically divided into two regimes - photon counting, where the rate of detected photons is small compared to the timing resolution of the detector and individual photoelectron pulses do not overlap, and signal integration, for light sources of higher intensities where individual photoelectron signals cannot be distinguished. In the latter case, for applications in which the resolution of the signal plays an important role, such as scintillation spectroscopy or pulse shape discrimination, it is critical to obtain an accurate estimate of the total number of generated photoelectrons, as well as the relative width of the single photoelectron pulse, since these are often the dominant contributors to the resolution of the signal. The response of a PMT is therefore typically calibrated relative to the mean of the charge distribution corresponding to a single detected photon, or equivalently, a single photoelectron (SPE). The calibration of the PMT SPE response is also necessary in order to combine the output signals from several different PMTs operating at different gains.

The standard method to perform such a calibration is to use an extremely low intensity light source such that the probability of generating more than a single photoelectron within the time resolution of the detector is negligible. The output spectrum of the integrated signal is then fit with a parameterized analytical model of the SPE response, in order to obtain the mean and variance for each individual PMT. The difficulty of such a method lies in the choice of the analytical model. Elec-

tron multiplication within the dynode chain is a branching process where the output charge distribution at the PMT anode depends on the secondary electron emission probability at each dynode. For typical photoelectrons generated at the photocathode, the most commonly used approximation is a standard Gaussian distribution [1], where the mean of the single photoelectron distribution is simply taken as the peak, though more complicated models such as [2, 3] are also used to more accurately model the electron cascade process. Additionally, a large variety of sub-optimal trajectories of electrons through the PMT dynodes are also possible. For example, a photon may pass through the cathode and directly strike the first dynode [4, 5], a photoelectron may inelastically backscatter off the first dynode [5, 6] or skip a dynode stage [7]. Such trajectories often lead to under-amplified photoelectron signals, increasing the component of the SPE spectrum with charge lower than that at the peak. Since these under-amplified photoelectrons are generated during normal operation and contribute to the total integrated signal, they should be included when estimating the mean and variance of the SPE response. Under-amplified photoelectrons can account for as much as 20% of the total photoelectron spectrum in some models of PMTs, decreasing the mean of the SPE response by 10-20% relative to the peak charge [8, 9]. Ignoring the contribution of under-amplified photoelectrons can lead to an underestimation of the number of detected photoelectrons and an incorrect estimation of the resolution.

The true shape of the under-amplified component is often difficult to determine due to the large overlap with contributions from electronics noise. Several authors have proposed adding additional analytical components to the fit function of the single photo-

electron response, including a falling exponential, and additional Gaussian components [9, 10]. However, the relative weight and shape of the under-amplified component can vary with the type of photocathode and dynode structure, and can even differ for individual PMTs of the same model and gain [4, 8]. Thus it is often difficult to construct an analytical parameterization of the single photoelectron spectrum that is suitable for a range of PMTs and conditions.

In this work we present a simple statistical method to calibrate the single photoelectron response of a photomultiplier tube without making any assumptions on the shape of the single photoelectron spectrum. Rather than using an analytical model, we rely on the known distribution of photoelectrons produced by a laser pulse to obtain the calibration parameters directly from the spectrum itself, without requiring a fit. The general statistical nature of the method allows it to be applied to any kind of photomultiplier tube with a wide range of illumination levels, while only requiring a pulsed laser light source, a device that is already commonly implemented in scintillation detectors.

II. METHOD

The single photoelectron calibration method presented here focusses on accurately estimating the mean and variance of the single photoelectron distribution at the PMT output, including contributions from under-amplified photoelectrons, without making any assumptions about the shape of the distribution. For most experimental purposes, knowledge of the higher moments, or the entire functional form of the single photoelectron response is not required. The linearity of the PMT ensures that as the number of detected photoelectrons increases, by the central limit theorem (CLT), the response to multiple photoelectrons quickly converges to a Gaussian distribution that is completely described by the first two central moments of the single photoelectron response. This is illustrated in Figure 1, where it can be seen that even for a heavily skewed single photoelectron distribution with a large fraction of under-amplified photoelectrons, the response to $n \geq 5$ photoelectrons (PE) is to a very good approximation Gaussian, with a mean and variance n times that of the entire SPE distribution. Even though the distribution converges to a Gaussian for large number of photoelectrons, it is critical to include the under-amplified component in the estimate of the mean and variance in order to obtain the correct estimate of the photoelectron statistics in the signal. For example, if one were to calibrate the SPE mean as simply the peak position of the SPE distribution in the top left panel of Figure 1, one would incorrectly underestimate the number of photoelectrons in the other panels by the ratio of the peak position to the true mean position (i.e. a factor of 1.25). We

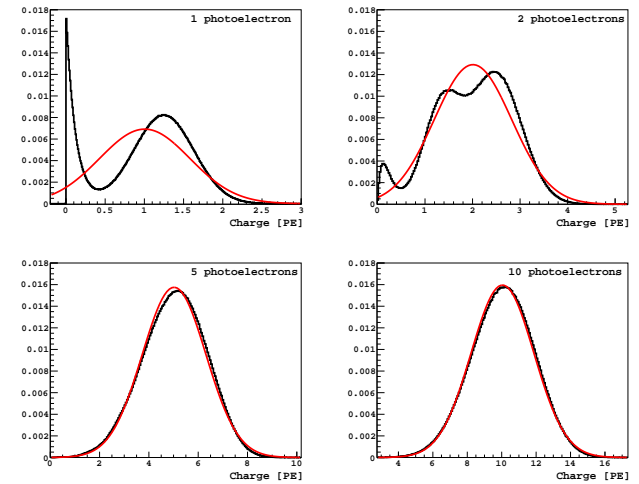


FIG. 1. Black: Simulated charge distribution of 1, 2, 5 and 10 photoelectrons for a PMT with a large component of under-amplified photoelectrons. Background noise was not included in the simulation. Red: Gaussian distribution with the same mean and variance as the PMT charge distribution for comparison.

note that the above considerations also apply when the light is distributed over an array of photomultipliers, and the total signal is obtained by summing the output of all the PMTs. In this case, even though the single photoelectron response of the individual PMTs are not necessarily identical, variants of the classical CLT typically ensure convergence to a Gaussian distribution. Thus, for scintillation signals that produce more than 5 PE on average, the contribution of the photomultiplier response is determined by only the first two central moments of the single photoelectron distribution. For smaller signals, the knowledge of the mean and variance are still necessary for calibration, and are still accurately estimated by the method described in this paper, though higher moments may also need to be calculated to fully model the shape of the detector response.

In order for the description of the method to be clear, we must first briefly describe the corresponding experimental setup. A low intensity, pulsed laser is used to illuminate the PMT to be calibrated. The laser is externally triggered and for each trigger the PMT output is digitized at the time corresponding to the expected anode output signal. We stress that in this setup the PMT's output for every trigger is recorded, even if no visible signal is observed. This ensures that no low amplitude photoelectrons are missed.

For every trigger, there are two contributions to the total measured charge q , one from the background noise that is always present in the system, even in the absence of a photoelectron signal, and one associated with the presence of a photoelectron signal. The total integrated charge is simply the sum of these two contributions, which, by definition, are independent. We will denote the probability distribution of the total inte-

grated charge as $T(q)$, and the background and signal probability distributions as $B(q)$ and $S(q)$ respectively. It then follows that

$$T(q) = B(q) * S(q) \quad (1)$$

where $*$ indicates a convolution of the two distributions. For independent random variables, the first two moments are additive, and hence

$$E[T] = E[B] + E[S] \quad (2)$$

$$V[T] = V[B] + V[S] \quad (3)$$

where $E[X]$ and $V[X]$ denote the mean and variance of the distribution X respectively, and we have omitted the domain of the distributions for clarity. The signal charge distribution can be written in terms of the number of photoelectrons p produced

$$S(q) = \sum_{p=0}^{\infty} S(q|p)L(p) \quad (4)$$

where $L(p)$ is the discrete probability distribution of the number of photoelectrons produced in a single laser pulse. Assuming that the PMT response is linear, we can write the multi-photoelectron response as the repeated convolution of the single photoelectron response, which we shall denote as $\psi(q) \equiv S(q|p=1)$

$$\begin{aligned} S(q|p) &= \psi(q) * \dots \text{(p convolutions)} \dots * \psi(q) \\ &\equiv \psi^p(q) \end{aligned}$$

where $\psi^0(q) \equiv \delta(0)$. We can now write the signal probability distribution as

$$S(q) = \sum_{p=0}^{\infty} \psi^p(q)L(p) \quad (5)$$

Using the above, one can calculate the mean and variance of the signal:

$$E[S] = E[\psi] \cdot E[L] \quad (6)$$

$$V[S] = V[\psi] \cdot E[L] + E^2[\psi] \cdot V[L] \quad (7)$$

Finally, we can substitute the above in Eqs. 2 and 3 to obtain the first two central moments of the single photoelectron response $\psi(q)$

$$E[\psi] = \frac{E[T] - E[B]}{E[L]} \quad (8)$$

$$V[\psi] = \frac{V[T] - V[B] - E^2[\psi] \cdot V[L]}{E[L]} \quad (9)$$

As can be seen from the above equations, in order to obtain the mean and variance of the single photoelectron distribution, one needs to know the mean and variance of the photoelectron distribution $L(p)$.

For an ideal laser emitting coherent light in a single mode, the distribution of the number of photons follows a Poisson distribution [11], with the variance equal to the mean. If the light is then attenuated by filters such that each photon independently has the same probability to pass through, the output photon distribution will also follow a Poisson distribution with a reduced mean. Even in the case where the emitted laser light is not perfectly Poissonian, it can be shown that after strong attenuation the output photon distribution approaches a Poisson distribution. Explicitly, if the initial laser photon distribution has a ratio of the variance to the mean, defined as the Fano factor [12], F_i , then after attenuation by a factor η ($0 \leq \eta \leq 1$), the Fano factor F_o of the output photon distribution is

$$F_o = 1 + \eta(F_i - 1)$$

Thus even for non-ideal lasers, if the output is strongly attenuated ($\eta \ll 1$), $F_o \approx 1$ and the variance approaches the mean, as for a Poisson distribution. Similarly, the expectation value for low numbers of output photons can also be shown to converge to those of a Poisson distribution [13, 14]. Given these considerations, we can assume that the distribution of photons from a strongly attenuated laser light source follows a Poisson distribution. Since the conversion from photons to photoelectrons can also be considered a random attenuation process, the distribution of photoelectrons produced at the photocathode is also Poissonian. We can therefore further simplify Eq. 9 by setting the variance of the photoelectron distribution equal to the mean, $V[L] = E[L]$, to get:

$$V[\psi] = \frac{V[T] - V[B]}{E[L]} - E^2[\psi] \quad (10)$$

Before discussing the method to estimate the parameters on the right hand side of Eq's (8) and (10) it is worthwhile to explicitly list some of the assumptions made above and compare them to other methods of single photoelectron calibration.

- Unlike fitting methods, we have not assumed any functional form for the single photoelectron response. The above equations are valid for any SPE distribution with no assumptions about the shape or amplitude of the under-amplified photoelectron distribution.
- Similarly, we have also made no assumption about the shape of the background noise distribution, which is determined by the specific electronics used and the background noise present in the setup.
- We have assumed that the PMT and any associated electronics respond linearly to the number of photoelectrons. In the typical regime used by this method, fewer than 20 PE are produced in each

laser pulse, which is well within the linear range of most PMTs.

- The above formulation divides the contributions of the total charge into two categories, background and signal. The background distribution accounts for all signals that are independent of the photoelectron production by the laser. This includes any noise from the electronics, the trigger and the pulsing of the laser (which occurs for every trigger) as well as dark count signals produced by thermionic emission from the photocathode and dynode chain. The signal distribution is assumed to only include contributions that are linear with the number of laser-induced photoelectrons. In certain experimental setups, there may be contributions that do not fall into either category. For example, noise from a discriminator firing (when the signal is above a certain threshold) may only occur when the laser light produces a signal, but it does not increase as the number of photoelectrons increases. In such cases, as with other calibration methods, care must be taken to account for these contributions in the total charge distribution.

III. PARAMETER ESTIMATION

As can be seen from Eq's (8) and (10), in order to determine the first two central moments of the SPE response we need to evaluate the first two central moments of the total charge distribution and the background distribution, as well as the mean number of photoelectrons produced in each trigger. Since we do not have prior knowledge of the true underlying distributions, we will estimate the moments from a data sample of N triggers.

The central moments of the total charge distribution can be directly obtained by calculating the mean and variance of the measured PMT output spectrum in the presence of the laser. An example of this spectrum can be seen in black in Figure 4 along with the mean and variance. This is typically the spectrum that is used to fit the single photoelectron response.

There is often an overlap of the background distribution and the signal distribution of under-amplified single photoelectrons. This makes it difficult to cleanly determine the mean and variance of the background in the presence of the laser signal. The simplest method to measure the background spectrum is to take an independent data set (which we will refer to as "blank", as opposed to "laser") and block any laser light from reaching the PMT, while leaving the laser on. This excludes signals associated with the laser light, while including any possible electronics noise produced by the pulsed laser. For simplicity we will assume that the same number of triggers N are acquired for the

blank and the signal distributions. An example background distribution used to calculate the mean and variance is shown in red in Figure 4.

The only parameter that is not straightforward to estimate is the mean number of laser-induced photoelectrons produced in each trigger, $E [L]$, which we shall refer to as occupancy. As discussed previously, the number of photoelectrons produced follows a Poisson distribution, which can be written as

$$L(p) = \frac{\lambda^p e^{-\lambda}}{p!} \quad (11)$$

$$\lambda \equiv E [L] = V [L] \quad (12)$$

The occupancy λ is directly related to the probability of producing zero laser-induced photoelectrons,

$$\lambda = -\ln (L(0)) \quad (13)$$

which can be estimated from the number of sample triggers with zero laser-induced photoelectrons (zero-pe triggers), N_0 , and the total number of sample triggers N

$$\hat{\lambda} = -\ln (\hat{N}_0 / N) \quad (14)$$

where $\hat{\lambda}$ and \hat{N}_0 denote the estimates of the occupancy and number of zero-pe triggers from the data sample taken respectively.

There are several different techniques that can be used to estimate the value N_0 and the optimal method will depend on the nature of the signal and background distributions. For example, if the temporal shape of the PMT output pulse is known, and the triggers are individually recorded, one can assign a likelihood for the presence of a laser-induced signal to each individual trigger. For the purposes of this paper, we will restrict ourselves to a very simple algorithm, whose statistical and systematic uncertainties can be estimated analytically.

We will use the fact that we have access to a pure sample of zero-pe events from the background distribution in the blank data and hence have empirical information about the shape of the zero-pe distribution. Since triggers which contain a non-zero number of laser-induced photoelectrons typically have a higher charge output than triggers that only contain background noise, we can take the laser output distribution and place a threshold cut at low charge values (see red dashed line in Figure 5) such that the fraction of non-zero-pe triggers that fall below the cut is negligible (this will be quantified later). Let the number of triggers that fall below the cut in the laser data set be A_S , which we will assume are only zero-pe triggers. In order to account for the remaining number of zero-pe triggers that fall above the cut, we calculate the fraction of the blank distribution that falls below the cut and re-correct our measured number of laser triggers below the cut by

that fraction. If the fraction of blank triggers that fall below our cut is A_B/N , then our estimate for N_0 is

$$\widehat{N}_0 = A_S \cdot \frac{N}{A_B} \quad (15)$$

IV. PARAMETER UNCERTAINTIES

In order to find the optimal operating parameters for the laser intensity and number of triggers, it is useful to calculate the statistical and systematic uncertainties corresponding to the estimate of the moments from the finite data sample.

From Eq (8) we can calculate the statistical uncertainty on the single photoelectron mean as

$$V \left[\widehat{E} [\psi] \right] = \frac{V \left[\widehat{E} [T] \right] + V \left[\widehat{E} [B] \right] + E^2 [\psi] \cdot V \left[\widehat{E} [L] \right]}{E^2 [L]} \quad (16)$$

where $\widehat{E} [X]$ denotes the estimated mean, *i.e.* the estimate of the mean of the distribution X from the finite data sample taken.

Since the mean of the total charge distribution, $\widehat{E} [T]$, is evaluated by calculating the arithmetic mean of the distribution, the statistical uncertainty on the estimate is simply the standard error on the mean

$$V \left[\widehat{E} [T] \right] = \frac{V [T]}{N} \quad (17)$$

where N is the number of sample triggers. Using Eq (10), one can write

$$V \left[\widehat{E} [T] \right] = \frac{E [L] \cdot (E^2 [\psi] + V [\psi]) + V [B]}{N} \quad (18)$$

Similarly to $\widehat{E} [T]$, the uncertainty on the estimate of $\widehat{E} [B]$ is simply the standard error on the mean

$$V \left[\widehat{E} [B] \right] = \frac{V [B]}{N} \quad (19)$$

If the true fraction of zero-pe triggers that fall below the threshold cut is denoted as f , such that $f \equiv E [A_B/N]$ the statistical uncertainty in the estimate of the occupancy can be written as (see Appendix A)

$$V \left[\widehat{\lambda} \right] \approx \frac{(e^\lambda + 1 - 2f)}{fN} \quad (20)$$

Combining the individual statistical uncertainties from Eqs (18), (19) and (20) into Eq (16), we get

$$V \left[\widehat{E} [\psi] \right] \approx \frac{\lambda(E^2 [\psi] + V [\psi]) + 2V [B]}{N\lambda^2} + \frac{E^2 [\psi] (e^\lambda + 1 - 2f)}{fN\lambda^2} \quad (21)$$

For a given photomultiplier and background spectrum, the statistical uncertainty on the single photoelectron mean as determined by this method decreases as the number of trigger samples N increases and is smallest for occupancies $\lambda \sim 2$ PE/trigger.

The dominant systematic uncertainty arises from the evaluation of the occupancy. The estimation of the occupancy is made under the assumption that the number of non-zero-pe triggers falling below the threshold cut is negligible. However measurements of signals from photomultiplier tubes operated at high gain have shown contributions from under-amplified photoelectrons of arbitrarily small charge [4, 8]. Triggers with a laser-induced photoelectron that produces a very small integrated charge can fall below the threshold cut and be incorrectly included in the calculated number of zero-pe triggers \widehat{N}_0 . This leads to systematic decrease in the estimated occupancy $\widehat{\lambda}$, and correspondingly a systematic increase in the estimated single photoelectron mean.

The number of non-zero-pe triggers, l , leaking below the threshold cut can be reasonably expected to be proportional to the number of events that produce exactly one photoelectron, since the probability of two or more photoelectrons producing a combined signal that falls below the threshold cut should be negligible. One can then write the mean number of leakage events l as

$$l = k \cdot N \cdot L(1) \quad (22)$$

$$= k \cdot N \cdot \lambda \cdot L(0) \quad (23)$$

where k is the fraction of all triggers with exactly one laser-induced photoelectron, whose total charge falls below the threshold cut. This translates into a biased estimate of the single photoelectron mean $\widehat{E} [\psi]$ (see Appendix B)

$$E \left[\widehat{E} [\psi] \right] \approx E [\psi] \cdot \left(1 + \frac{k}{f} \right) \quad (24)$$

Thus, in order to minimize the systematic bias in the estimate of the single photoelectron mean, the value of the threshold cut must be chosen such that k/f (the ratio of the fraction of the single photoelectrons below the threshold cut to the fraction of the background spectrum below the cut) is small.

The uncertainty in the estimation of the single photoelectron variance is difficult to calculate analytically and was evaluated using the simulations described in Section VI.

V. EXPERIMENTAL METHOD

In order to test the calibration method described above we have used the experimental setup illustrated in Figure 2. A Hamamatsu R11410 3" photomultiplier with a box and linear-focused dynode structure [15], total divider resistance of $37\text{ M}\Omega$ and the recommended

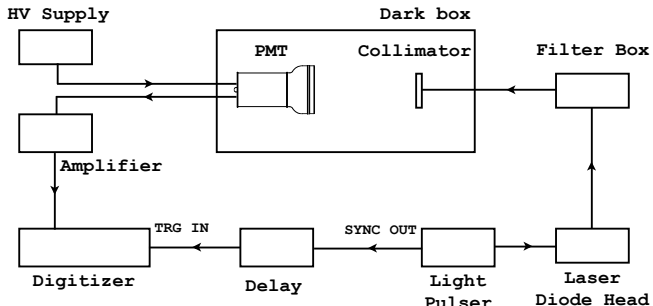


FIG. 2. Schematic diagram of the experimental setup used to measure the single photoelectron spectrum with a pulsed laser light source.

voltage distribution ratio was placed in a custom-made metal darkbox that featured a continuous conducting surface to reduce the effect of electrical noise. The PMT was illuminated by a collimated optical fibre that carried light from a fast pulsed laser diode (Hamamatsu PLP-10-040C [15]) which we will henceforth refer to as a laser. The laser pulses had a typical width of 60 ps (FWHM) and a wavelength of 405 nm. The intensity of the light incident on the PMT was varied by placing different neutral density filters along the laser path. For all data sets acquired, the combined attenuation factor η of the filters was kept $\leq 10^{-5}$, in order to ensure that the photon distribution was Poissonian. The anode of the PMT was terminated with a 50Ω resistor and connected to a custom fast amplifier with a 10x gain. The output of the amplifier was then sent to a 12 bit, 250 MHz CAEN V1720 digitizer [16]. The digitizer was externally triggered by the synchronous output of the laser which was delayed by 500 ns with respect to the optical signal, to avoid the PMT output overlapping with noise produced by the digitizer triggering. For each trigger a 1 μ s digitized waveform was recorded and stored for analysis offline.

For each configuration of light intensity and PMT voltage that was studied, two data sets of $N = 500,000$ triggers were acquired at a trigger rate of 1 kHz. A “laser” data set was acquired with the optical fibre connected such that the laser light illuminated the PMT and another “blank” data set was acquired with the optical fibre disconnected before the filter box, and the fibre feedthrough capped. In order to ensure that the noise levels remained the same for both the laser and blank data, all the electronics were kept in the same operating conditions for both runs. As a consistency check, for a few configurations, a blank data set was taken before and after the laser data set and the integrated charge distribution for the two blank data sets were compared using the Kolmogorov-Smirnov test. In all cases, the integrated charge spectrum of the blank data sets were found to be compatible (p -value > 0.1).

The event reconstruction required for this calibration method is straightforward. The expected time win-

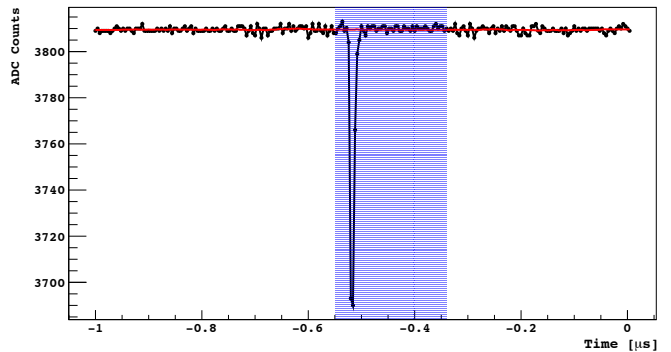


FIG. 3. Example of a digitized PMT signal within a sample trigger window, acquired during a laser data set. The black points indicate the digitized waveform, with the red line showing the estimated baseline. The shaded blue region indicates the fixed laser time window chosen for integration. The negative pulse in the laser time window likely indicates the presence of a laser-induced photoelectron signal.

dow for the laser-induced PMT signal is first identified empirically by averaging together all the waveforms acquired during a laser data set and selecting a 208 ns time window that included the entire laser-induced signal. Outside of the laser time window a baseline is calculated for each individual waveform using a moving average of ± 20 ns around each sample. The baseline within the laser time window is then linearly interpolated using the samples on either side of the window. This method ensures that the baseline is evaluated in the same way regardless of whether or not a laser signal is present. A sample waveform along with the defined laser time window and estimated baseline is shown in Figure 3.

The integral (inverted to account for the negative PMT pulses) of the baseline-subtracted waveform over the defined laser time window is calculated for each trigger. Figure 4 shows the distribution of the integral for a laser and blank data set, acquired at a PMT voltage of 1700 V ($\approx 1.6 \times 10^7$ gain) and a filter attenuation of 5×10^{-6} . In both distributions the peak centered at zero is primarily due to fluctuations of the noise about the estimated baseline with no photoelectron signal present. The peak at 400 count·samples in the laser data is due to fully amplified single photoelectrons from the photocathode, and a peak due to two fully amplified photoelectrons at 800 count·samples is also visible. The small peak at 400 count·samples in the blank data is due to dark noise photoelectrons and possibly small amounts of stray light entering the darkbox ($< 0.2\%$ of triggers) that accidentally fall within the laser time window. The inclusion of these events in the blank data allows us to correctly account for their presence in the laser data and exclude them from the estimation of the single photoelectron mean, since the spectrum of dark noise photoelectrons do not necessarily follow the same distribution as photon-induced photoelectrons [6, 9].

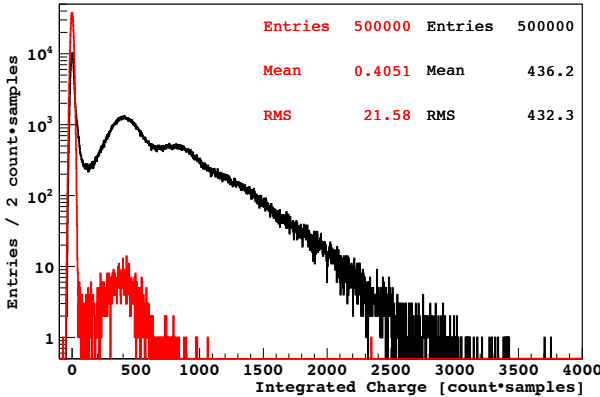


FIG. 4. Black: Integrated charge spectrum for a laser data set acquired at a PMT voltage of 1700 V and an estimated occupancy of 1.35 photoelectrons/trigger. Red: Integrated charge spectrum for a blank data set taken at the same settings as the laser data set, but with the optical fibre disconnected.

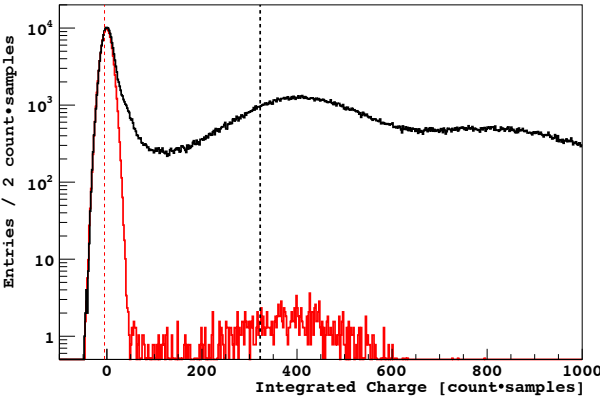


FIG. 5. Same data as in Figure 4, with the blank data spectrum scaled to match the laser data spectrum using the estimated occupancy. The red vertical line indicates the position of the threshold cut used to estimate the occupancy. The black vertical line indicates the value of the estimated single photoelectron mean.

Figure 5 focuses on the low charge region of the laser and blank data set shown in Figure 4, with the blank spectrum scaled to match the number of zero laser-induced photoelectron triggers in the laser spectrum using the estimated occupancy. The occupancy was estimated using the method described in Section III, where a threshold cut was placed such that the fraction of the blank data set that falls below the cut is $f = 0.333$ (red dashed line in Figure 5). As discussed in Section IV, the position of the threshold cut was chosen to keep the fraction of the single photoelectron triggers falling below the cut small, while still maintaining enough statistics below the cut in the blank spectrum to accurately estimate the occupancy. The placement of the cut below an integrated charge of zero implies that only very small single photoelectron signals, which when summed with the background noise lead to an

overall negative charge (after baseline subtraction), will fall below the threshold cut.

It can be seen in Figure 5 that between 50 and 100 count·samples the excess of the laser spectrum above the blank spectrum differs significantly from a Gaussian tail, indicating the presence of a distinct population of under-amplified photoelectrons with low integrated charge. The mean of the single photoelectron distribution, as estimated by the method described in this paper, is shown by the black dashed line in Figure 5. As one would expect, the presence of under-amplified photoelectrons with lower output charge pushes the estimated mean distinctly below the peak of the fully-amplified single photoelectron distribution. For the PMT and operating gain described above, the estimated mean of the entire single-photoelectron distribution, including under-amplified photoelectrons, is $\approx 80\%$ of the peak of the fully-amplified single-photoelectron distribution.

In order to study the robustness of the method with respect to intensity of laser light used, several data sets were taken with the PMT supplied at a constant voltage, but with different filter attenuation. Since different numbers and combinations of filters were used to obtain different light intensities, the observed occupancy did not directly scale with the filter attenuation used, due to reflections between filters. Figure 6 shows the obtained laser spectra, where the distributions have been normalized to have the same number of zero-pe triggers, based on the estimated occupancy. The results for the estimated single photoelectron mean and standard deviation, $\widehat{SD}[\psi] \equiv \sqrt{\widehat{V}[\psi]}$, are shown in Table I. It can be seen that unlike most commonly used fitting methods which require a very low occupancy (due to difficulties in calculating and fitting analytical functions for two or more photoelectrons), this method produces consistent results for the single photoelectron mean, with statistical uncertainties below 2%, over a range of laser intensities that span from 0.2 to 2.4 PE/trigger. While the experimental data was limited by the set of available filters, Eq. 21 indicates that for the parameters of this experimental setup, the method has a precision of better than 3% for occupancies spanning nearly two orders of magnitude from 0.1 to 9.5 PE/trigger. This is especially useful for large detectors that contain an array of photomultiplier tubes, where a uniform illumination of the PMTs with optical fibers may not be possible.

Due to dynamic range limitations in many experimental setups, it is often not possible to run PMTs at high gain values. Running at lower gain often results in the under-amplified photoelectron spectrum falling under the zero-pe background, as shown in Figure 7 where laser spectra for data sets were taken at a constant laser intensity but varying voltage applied to the PMT.

Since the method described above uses a simple

Attenuation η	Occupancy $\hat{\lambda}$	SPE Mean		SPE Std. Dev. $\widehat{SD}[\psi]$	SPE Rel. Std. Dev. $\frac{\widehat{SD}[\psi]}{\widehat{E}[\psi]}$
		$\widehat{E}[\psi]$	[count·samples]		
		[PE/trigger]	[count·samples]		
1E-5	2.395 ± 0.008	324 ± 1	185 ± 2	0.571 ± 0.007	
5E-6	1.351 ± 0.005	323 ± 1	184 ± 2	0.571 ± 0.007	
1E-6	0.206 ± 0.003	330 ± 5	180 ± 7	0.55 ± 0.03	
1E-7	0.012 ± 0.003	390 ± 90	140 ± 30	0.4 ± 0.1	

TABLE I. Results for the estimated occupancy, single photoelectron mean and standard deviation for data acquired at a fixed PMT voltage (1700 V), with different optical filters to vary the intensity of laser light.

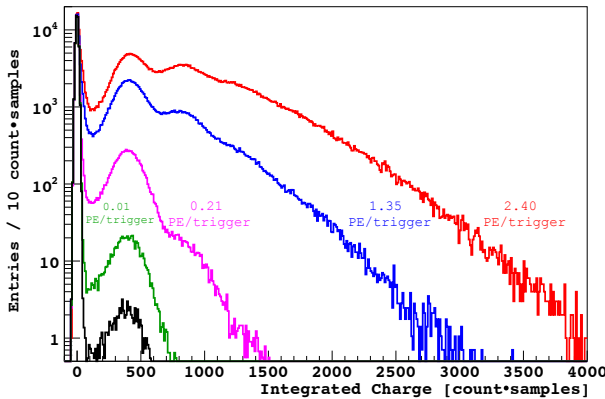


FIG. 6. Integrated charge spectra for laser data sets acquired at 1700 V with varying light intensity ($\hat{\lambda} = 2.40, 1.35, 0.21$ and 0.01 photoelectrons/trigger), along with the corresponding blank data set shown in black for comparison. The spectra are all scaled to have the same number of zero-pe triggers using the estimated occupancy.

threshold cut to estimate the occupancy, the overlapping of the noise and under-amplified photoelectrons makes it difficult to accurately estimate the occupancy and hence the single photoelectron mean and variance. The results for the estimated single-photoelectron mean and variance are shown in Table II, where it can be seen that the estimated occupancy steadily decreases as the gain decreases. While there may be some small loss of photomultiplier efficiency at lower voltages due to inefficient focussing in the dynode structure, as we will see in Section VI, the decrease in estimated occupancy is consistent with the expected systematic bias described in Section IV. More sophisticated algorithms that rely on other parameters to estimate the occupancy will likely be less biased at low gains.

If one assumes that the PMT efficiency remains constant for all the voltages applied, one can fix the occupancy to the value obtained at the highest gain, where the systematic bias is least. Table III shows the results obtained by using the value of the occupancy obtained

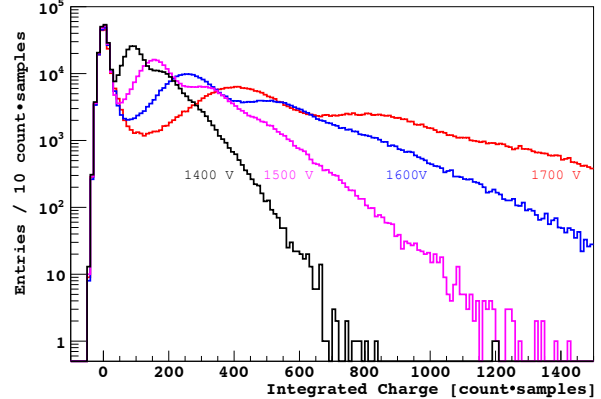


FIG. 7. Integrated charge spectra for laser data sets acquired at a fixed laser intensity ($\hat{\lambda} = 1.35$ photoelectrons/trigger) with varying PMT voltage (1400 V, 1500 V, 1600 V, 1700 V).

at the highest gain to estimate the single photoelectron moments at lower PMT voltages. The results obtained using this method give more consistent values for both the single photoelectron relative variance and the ratio of the single photoelectron peak to mean. Thus, for applications in which the photomultiplier is required to be calibrated at low gain, it is recommended to estimate the occupancy by temporarily running the PMT at a higher gain, while keeping the laser intensity constant. The value of the occupancy can then be used to calculate the single photoelectron mean and variance at the desired operating gain. If it is not possible to temporarily increase the PMT gain, the systematic bias in the estimated single photoelectron moments can be estimated using simulations, as discussed in the following section. As we will see, for the given experimental setup and simple algorithm used to estimate the occupancy, the bias at the lowest operating gain is still less than 10% and the result obtained is always more accurate than using a simple Gaussian fit.

PMT HV	Occupancy	SPE Mean	SPE Std. Dev.	SPE Rel. Std. Dev.	SPE Mean/Peak
	$\hat{\lambda}$	$\hat{E} [\psi]$	$\hat{SD} [\psi]$	$\frac{\hat{SD} [\psi]}{\hat{E} [\psi]}$	
[Volts]	[PE/trigger]	[count·samples]	[count·samples]		
1400	1.257 ± 0.005	76.9 ± 0.3	35.4 ± 0.4	0.460 ± 0.006	0.854 ± 0.005
1500	1.289 ± 0.005	127.3 ± 0.5	64.0 ± 0.7	0.503 ± 0.007	0.815 ± 0.004
1600	1.324 ± 0.005	204.3 ± 0.8	111 ± 1	0.543 ± 0.006	0.803 ± 0.004
1700	1.351 ± 0.005	323 ± 1	184 ± 2	0.571 ± 0.007	0.791 ± 0.004

TABLE II. Estimated occupancy, single photoelectron mean and standard deviation for data acquired at a fixed light intensity (1.35 PE/trigger), with varying PMT voltages to vary the single photoelectron gain.

PMT HV	Occupancy	SPE Mean	SPE Std. Dev.	SPE Rel. Std. Dev.	SPE Mean/Peak
	$\hat{\lambda}$	$\hat{E} [\psi]$	$\hat{SD} [\psi]$	$\frac{\hat{SD} [\psi]}{\hat{E} [\psi]}$	
[Volts]	[PE/trigger]	[count·samples]	[count·samples]		
1400	1.351 ± 0.005	71.5 ± 0.3	39.4 ± 0.4	0.551 ± 0.008	0.795 ± 0.004
1500	1.351 ± 0.005	121.5 ± 0.5	68.0 ± 0.7	0.560 ± 0.007	0.778 ± 0.004
1600	1.351 ± 0.005	200.2 ± 0.8	114 ± 1	0.569 ± 0.007	0.786 ± 0.004
1700	1.351 ± 0.005	323 ± 1	184 ± 2	0.571 ± 0.007	0.791 ± 0.004

TABLE III. Estimated single photoelectron mean and standard deviation for data acquired at a fixed light intensity (1.35 PE/trigger), with varying PMT voltages to vary the single photoelectron gain. For all data sets the occupancy was set to the occupancy estimated at the highest gain, where the systematic bias of the method is expected to be smallest.

VI. MONTE CARLO

In order to verify that the single photoelectron calibration method described in this paper works accurately not only for the specific photomultiplier and conditions studied in the experimental setup, but also for different single photoelectron spectra, light intensities, and PMT gain, a Monte Carlo generator was written to simulate laser-induced PMT pulses and overlay them on waveforms taken during blank data sets. The simulated events were then processed in the same manner as the experimental data and the estimated single photoelectron moments, averaged over a large number of trials, were compared to the simulated inputs as a function of the gain, occupancy and shape of the single photoelectron spectrum.

The simulation of each event in a given configuration begins by drawing a random number of photoelectrons from a Poisson distribution with a fixed mean corresponding to the desired occupancy. The integrated charge corresponding to each photoelectron was then independently drawn from a spectrum. Since the true shape of the single photoelectron charge spectrum is not known, three different spectra were studied. The first spectra was derived from the experimental data, with a Gaussian peak representing the fully amplified

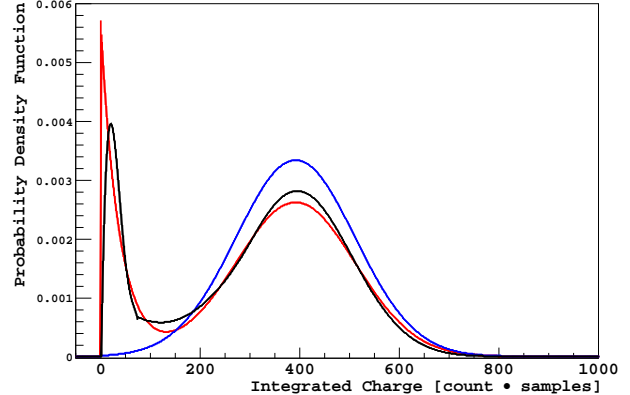


FIG. 8. Different integrated charge spectra used as single photoelectron distributions in the Monte Carlo simulations. Blue: Gaussian distribution. Black: Gaussian distribution plus an under-amplified component whose shape was obtained from the difference of the experimentally measured laser and blank spectra. Red: Gaussian distribution with an exponential under-amplified distribution.

photoelectron distribution and a under-amplified distribution that was obtained by subtracting the scaled blank spectrum from the events acquired at highest gain and occupancy. This empirically derived spec-

trum, shown in black in Figure 8, displays a prominent peak at low charge values, very similar to the shapes obtained in other experimental setups for a variety of different photomultiplier tubes [4, 8, 10]. We then considered two other shapes as potential extreme cases: a simple Gaussian truncated at zero, representative of a single photoelectron distribution without any contribution from under-amplified photoelectrons, and a Gaussian with an under-amplified distribution that rises exponentially at low charge values [9]. For the latter two distributions, shown in blue and red respectively in Figure 8, the shape of the spectrum was tuned to try and match the experimental data as best as possible. In order to simulate different gains, the spectra were linearly scaled such that the peak of the Gaussian matched the experimental data at each PMT high voltage value.

For each simulated photoelectron a temporal pulse is generated based on measurements of the average single photoelectron pulse shape. The integral of the pulse is scaled to equal the charge assigned to the photoelectron and the peak time is set to match the arrival time of the PMT signal in the experimental setup. The pulses corresponding to all the photoelectrons in a given trigger are then summed together and overlaid on top of a waveform taken during a blank data set taken in the same configuration, accounting for the discreteness of the ADC samples in time and amplitude. The use of the experimentally obtained waveforms from the blank data set allows us to accurately include all of the relevant effects such as noise, stray photoelectrons and dark current into the simulation. Each waveform is the processed identically to the experimentally obtained data in order to obtain the simulated laser spectra and estimate the single photoelectron mean and variance.

Using the results of the simulation, we studied the effects of the systematic bias described in Section IV for the three different single photoelectron spectra. At lower gains, the overlap of the under-amplified photoelectrons and the electronics noise increases, and the bias is expected to increase. For the simple occupancy estimation method described in this paper, the single photoelectron mean is expected to be biased upward by approximately a factor of $(1 + k/f)$ (where k/f is the ratio of the fraction of the single photoelectrons below the threshold cut to the fraction of the background spectrum below the cut). In Table V we report the results of the simulation for single photoelectron gain settings corresponding to the PMT HV supply values used in the experimental setup, and an occupancy of 1.35 PE/trigger. As expected, the systematic bias is directly proportional to the overlap of the single photoelectron spectrum with the noise. For the Gaussian spectrum there is no significant bias at all gains, while for the empirical spectrum obtained from the experimental measurements of the R11410, the bias varies from +1% to +8%, depending on the gain, consistent with the corre-

sponding k/f ratio. It should be noted that even in the worst case considered, with a exponentially increasing under-amplified spectrum at low gain, the systematic bias in the single photoelectron mean and standard deviation of +10% and -15% respectively is significantly lower than the bias one would obtain by ignoring the under-amplified electrons and only fitting the Gaussian component (+19% and -50% respectively).

In order to test the sensitivity of the method to the intensity of laser light, we simulated datasets at various occupancies, for all three different single photoelectron spectra at a gain equivalent to the experimental data taken at 1700 V. The results are shown in Table VII, where it can be seen that the calibration method provides results that are consistent with the simulated single photoelectron moments (after accounting for the small systematic bias discussed above). The statistical uncertainties on the single photoelectron mean and standard deviation for all three considered single photoelectron spectra are less than 3% and 4% respectively for occupancies ranging from 0.1 to 7.5 PE/trigger. This confirms the validity of the method for a wide range of PMT illumination.

VII. CONCLUSIONS

In this paper we have presented a simple new method to calibrate the single photoelectron response of photomultiplier tubes, taking into account the important contributions of under-amplified photoelectrons. Unlike conventional fitting methods, the proposed procedure determines the single photoelectron mean and variance statistically, without making any assumption about the underlying shape of the single photoelectron spectrum, and can thus be used to calibrate PMTs with various photocathode and dynode structures. Following the description of the method, we have outlined the procedure to estimate the required parameters and their uncertainties, and applied the method to experimental data acquired with a Hamamatsu R11410 photomultiplier. Additionally we have used a Monte Carlo simulation with experimentally measured noise levels to study the results of the method as a function of the single photoelectron spectrum, photomultiplier gain and light intensity. The method is found to accurately estimate the single photoelectron mean (variance) to better than 5% (6%) for all single photoelectron spectra considered, at PMT gain values above 1×10^7 . At lower gains, a systematic bias is present due to the overlap of the under-amplified spectra with the noise. For the experimental setup considered, the bias on the single photoelectron mean (variance) ranges from 0% (0%) to +10% (-15%) at a gain of 3.5×10^6 , depending on the single photoelectron spectrum. In all cases the bias is significantly less than other methods that ignore the contribution of under-amplified photoelectrons, and can likely be further reduced by the use of more sophisticated al-

Sim. Gain	Gaussian			Empirical			Gaussian + Exponential		
	$1 + \frac{k}{f}$	$E[\hat{E}[\psi]]$	$SD[\hat{E}[\psi]]$	$1 + \frac{k}{f}$	$E[\hat{E}[\psi]]$	$SD[\hat{E}[\psi]]$	$1 + \frac{k}{f}$	$E[\hat{E}[\psi]]$	$SD[\hat{E}[\psi]]$
3.5×10^6	1.0009	0.999 ± 0.003	0.004	1.075	1.079 ± 0.004	0.004	1.103	1.113 ± 0.004	0.004
5.9×10^6	1.0005	0.999 ± 0.003	0.004	1.045	1.045 ± 0.004	0.004	1.075	1.079 ± 0.003	0.004
9.8×10^6	1.0003	1.000 ± 0.003	0.004	1.021	1.021 ± 0.004	0.004	1.050	1.050 ± 0.004	0.004
1.6×10^7	1.0001	0.999 ± 0.003	0.004	1.010	1.009 ± 0.004	0.004	1.033	1.035 ± 0.004	0.004

TABLE IV. Simulation results for the estimated single photoelectron mean for a fixed occupancy (1.35 PE/trigger), with varying gain. Results are presented for all three simulated single photoelectron distributions with the first column indicating the analytically estimated fractional bias for each distribution and gain (see Section IV). The second column indicates the estimated fractional bias from the simulation compared to the true simulated value $E_{sim}[\psi]$, and the third column indicates the fractional statistical uncertainty (precision).

Sim. Gain	Gaussian		Empirical		Gaussian + Exponential	
	$E[\hat{SD}[\psi]]$	$SD[\hat{SD}[\psi]]$	$E[\hat{SD}[\psi]]$	$SD[\hat{SD}[\psi]]$	$E[\hat{SD}[\psi]]$	$SD[\hat{SD}[\psi]]$
3.5×10^6	1.00 ± 0.02	0.017	0.881 ± 0.007	0.008	0.848 ± 0.007	0.008
5.9×10^6	1.00 ± 0.02	0.018	0.936 ± 0.006	0.007	0.903 ± 0.005	0.007
9.8×10^6	0.99 ± 0.02	0.017	0.969 ± 0.006	0.006	0.938 ± 0.006	0.006
1.6×10^7	0.99 ± 0.02	0.018	0.984 ± 0.006	0.006	0.959 ± 0.006	0.006

TABLE V. Simulation results for the estimated standard deviation of the single photoelectron distribution for a fixed occupancy (1.35 PE/trigger), with varying gain. Results are presented for all three simulated single photoelectron distributions with the first column indicating the fractional bias (accuracy) compared to the true simulated value $SD_{sim}[\psi]$, and the second column indicating the fractional statistical uncertainty (precision).

gorithms to distinguish between signal and noise. The method also works well over a wide range of light intensities and is thus suitable for the calibration of arrays of photomultipliers in large detectors, where uniform illumination is not possible.

VIII. ACKNOWLEDGEMENTS

The authors would like to acknowledge helpful discussions with Jason Brodsky, Peter Meyers, and Alessandra Tonazzo during the development of this method. This work was supported in part by the Kavli Institute for Cosmological Physics at the University of Chicago through grant NSF PHY-1125897 and an endowment from the Kavli Foundation and its founder Fred Kavli.

Appendix A

The statistical uncertainty in the estimate of the occupancy λ (excluding any bias from non-zero-pe triggers leaking below the amplitude cut) can be evaluated by

first calculating the uncertainty in the number of zero-pe triggers $\widehat{N}_0 = A_S \cdot N / A_B$. Let the true fraction of zero-pe triggers be $L(0)$ and the true fraction of zero-pe triggers that fall below the cut be f . Then, for an ensemble of data sets with N triggers each

$$E[A_S] = NL(0)f; \quad V[A_S] = NL(0)f(1 - L(0)f) \\ E\left[\frac{N}{A_B}\right] \approx \frac{1}{f}; \quad V\left[\frac{N}{A_B}\right] \approx \frac{1-f}{Nf^3}$$

where we have used the fact that both A_S and A_B follow a binomial distribution and we have used a first-order Taylor expansion to estimate the mean and variance of the inverse of A_B . We can then write the mean and

Sim. Occ. λ	Gaussian		Empirical		Gaussian + Exponential	
	$E[\hat{E}[\psi]]$ $E_{sim}[\psi]$	$SD[\hat{E}[\psi]]$ $\hat{E}[\psi]$	$E[\hat{E}[\psi]]$ $E_{sim}[\psi]$	$SD[\hat{E}[\psi]]$ $\hat{E}[\psi]$	$E[\hat{E}[\psi]]$ $E_{sim}[\psi]$	$SD[\hat{E}[\psi]]$ $\hat{E}[\psi]$
0.10	0.99 ± 0.02	0.028	1.01 ± 0.02	0.029	1.04 ± 0.02	0.029
0.21	1.00 ± 0.01	0.014	1.01 ± 0.02	0.015	1.04 ± 0.02	0.015
1.35	0.999 ± 0.003	0.004	1.009 ± 0.004	0.004	1.035 ± 0.004	0.004
2.40	1.000 ± 0.004	0.003	1.008 ± 0.004	0.003	1.035 ± 0.004	0.003
5.00	1.000 ± 0.006	0.006	1.006 ± 0.006	0.006	1.032 ± 0.006	0.006
7.50	1.00 ± 0.02	0.014	1.00 ± 0.01	0.014	1.03 ± 0.01	0.013

TABLE VI. Simulation results for the estimated single photoelectron mean for a fixed gain (1.6×10^7), with varying occupancy. Results are presented for all three simulated single photoelectron distributions with the first column indicating the fractional bias (accuracy) compared to the true simulated value $E_{sim}[\psi]$, and the second column indicating the fractional statistical uncertainty (precision).

Sim. Occ. λ	Gaussian		Empirical		Gaussian + Exponential	
	$E[\hat{SD}[\psi]]$ $SD_{sim}[\psi]$	$SD[\hat{SD}[\psi]]$ $\hat{SD}[\psi]$	$E[\hat{SD}[\psi]]$ $SD_{sim}[\psi]$	$SD[\hat{SD}[\psi]]$ $\hat{SD}[\psi]$	$E[\hat{SD}[\psi]]$ $SD_{sim}[\psi]$	$SD[\hat{SD}[\psi]]$ $\hat{SD}[\psi]$
0.10	1.03 ± 0.08	0.153	0.96 ± 0.06	0.037	0.94 ± 0.05	0.037
0.21	0.97 ± 0.08	0.072	0.98 ± 0.02	0.019	0.94 ± 0.03	0.019
1.35	0.99 ± 0.02	0.018	0.984 ± 0.006	0.006	0.959 ± 0.006	0.006
2.40	0.99 ± 0.02	0.017	0.987 ± 0.005	0.006	0.959 ± 0.005	0.006
5.00	0.99 ± 0.03	0.031	0.988 ± 0.008	0.009	0.960 ± 0.007	0.008
7.50	0.96 ± 0.08	0.069	0.99 ± 0.02	0.018	0.96 ± 0.02	0.017

TABLE VII. Simulation results for the estimated standard deviation of the single photoelectron distribution for a fixed gain (1.6×10^7), with varying occupancy. Results are presented for all three simulated single photoelectron distributions with the first column indicating the fractional bias (accuracy) compared to the true simulated value $SD_{sim}[\psi]$, and the second column indicating the fractional statistical uncertainty (precision).

variance of \widehat{N}_0 and $\widehat{\lambda}$ as

Appendix B

$$E[\widehat{N}_0] \approx NL(0)$$

$$V[\widehat{N}_0] \approx NL(0) \left(\frac{1+L(0)}{f} - 2L(0) \right)$$

$$E[\widehat{\lambda}] \approx -\ln(L(0)) \\ = \lambda$$

$$V[\widehat{\lambda}] \approx \frac{\left(\frac{1+L(0)}{f} - 2L(0) \right)}{NL(0)} \\ = \frac{(e^\lambda + 1 - 2f)}{Nf}$$

Triggers with laser-induced single photoelectrons that fall below the amplitude cut lead to an overestimate of zero-pe triggers below the cut A_S and hence the estimated total number of zero-pe triggers \widehat{N}_0

$$E[A_S] = NL(0)f + l \\ = NL(0)(f + k\lambda)$$

$$E[\widehat{N}_0] \approx NL(0) \left(1 + \frac{k}{f} \cdot \lambda \right)$$

This translates into biased estimates of the occupancy $\widehat{\lambda}$ and the single photoelectron mean $\widehat{E}[\psi]$

$$\begin{aligned} E[\widehat{\lambda}] &= E[-\ln(\widehat{N_0}/N)] \\ &\approx \lambda - \ln\left(1 + \frac{k}{f} \cdot \lambda\right) \\ E[\widehat{E}[\psi]] &\approx E[\psi] \cdot \left(1 + \frac{k}{f}\right) \end{aligned}$$

where we have assumed that $k/f \ll 1$.

[1] E. Bellamy, G. Bellettini, J. Budagov, F. Cervelli, I. Chirikov-Zorin, M. Incagli, D. Lucchesi, C. Pagliarone, S. Tokar, F. Zetti, Absolute calibration and monitoring of a spectrometric channel using a photomultiplier, Nuclear Instruments and Methods in Physics Research Section A: Accelerators, Spectrometers, Detectors and Associated Equipment 339 (1994) 468 – 476.

[2] J. Prescott, A statistical model for photomultiplier single-electron statistics, Nuclear Instruments and Methods 39 (1966) 173 – 179.

[3] F. J. Lombard, F. Martin, Statistics of electron multiplication, Review of Scientific Instruments 32 (1961) 200–201.

[4] A. G. Wright, Method for the determination of photomultiplier collection efficiency, F, Appl. Opt. 49 (2010) 2059–2065.

[5] F. Kaether, C. Langbrandtner, Transit time and charge correlations of single photoelectron events in R7081 photomultiplier tubes, Journal of Instrumentation 7 (2012) P09002.

[6] S.-O. Flyckt, C. Marmonier, Photomultiplier tubes: principles and applications, Photonis, Brive, France, 2002.

[7] D. Carter, Photomultiplier Handbook: Theory, Design, Application, Lancaster, Pennsylvania: Burle Industries, Inc., 1980.

[8] J. de Haas, P. Dorenbos, Methods for accurate measurement of the response of photomultiplier tubes and intensity of light pulses, Nuclear Science, IEEE Transactions on 58 (2011) 1290–1296.

[9] R. Dossi, A. Ianni, G. Ranucci, O. Smirnov, Methods for precise photoelectron counting with photomultipliers, Nuclear Instruments and Methods in Physics Research Section A: Accelerators, Spectrometers, Detectors and Associated Equipment 451 (2000) 623 – 637.

[10] I. Chirikov-Zorin, I. Fedorko, A. Menzione, M. Pikna, I. Sykora, S. Tokar, Method for precise analysis of the metal package photomultiplier single photoelectron spectra, Nuclear Instruments and Methods in Physics Research Section A: Accelerators, Spectrometers, Detectors and Associated Equipment 456 (2001) 310 – 324.

[11] B. E. Saleh, M. C. Teich, Fundamentals of Photonics, volume 22, John Wiley & Sons, Inc., 1991.

[12] U. Fano, Ionization yield of radiations. ii. the fluctuations of the number of ions, Phys. Rev. 72 (1947) 26–29.

[13] Y. Hu, X. Peng, T. Li, H. Guo, On the Poisson approximation to photon distribution for faint lasers, Physics Letters A 367 (2007) 173 – 176.

[14] M. C. Teich, B. E. A. Saleh, Effects of random deletion and additive noise on bunched and antibunched photon-counting statistics, Opt. Lett. 7 (1982) 365–367.

[15] Hamamatsu photonics, Accessed: 11th September 2015. URL: <http://www.hamamatsu.com/us/en/index.html>.

[16] CAEN V1720 Digitizer, Accessed 11th September 2015. URL: <http://www.caen.it/csite/CaenProd.jsp?idmod=570&parent=11>.